

Compact and miniature snapshot imaging polarimeter

Haitao Luo,¹ Kazuhiko Oka,² Edward DeHoog,³ Michael Kudenov,¹
James Schiewgerling,¹ and Eustace L. Dereniak¹

¹College of Optical Science, University of Arizona, 1630 East University Boulevard, Tucson, Arizona 85721

²Division of Applied Physics, Graduate School of Engineering, Hokkaido University, Sapporo 060-8628, Japan

³Biomedical Engineering Program, University of Arizona, 1657 East Helen Street, Tucson, Arizona 85721

Received 7 May 2008; accepted 19 June 2008;
posted 9 July 2008 (Doc. ID 95874); published 19 August 2008

We present and demonstrate a compact and miniature snapshot imaging polarimeter camera; it is anticipated that such a camera can be scaled down to less than 1.5 cm. Two Savart plates are used at the pupil plane to generate multiple fringes to encode the full Stokes vector in a single image. A geometric ray model is developed to explain the system. The numerical simulation based on this model is presented. Finally, the validity of the device is demonstrated by showing experimental results. © 2008 Optical Society of America

OCIS codes: 120.2130, 120.5410, 260.5430.

1. Introduction

In remote sensing, bioscience, or other scientific areas, a compact or miniature imaging polarimeter that can be used to measure the state of polarization (SOP) of an object would be a powerful tool. For example, a surveillance imaging polarimeter would be valuable on small unmanned air vehicles. Likewise, an endoscopic imaging polarimeter could be easily inserted into a body cavity. These are challenging tasks for conventional polarimeters that use several rotating polarization elements to extract the complete Stokes vector of an object, as they are sensitive to vibration and contain more mechanical complexity. One technique that uses microretarder and polarizer arrays on the image plane has proved to achieve a compact device [1,2] although the sensitivity to fabrication errors and noise limits the accuracy. Another strategy demonstrated in monochromatic applications was the use of cascading birefringent prisms [3]. The fabrication difficulty of the tiny prisms is a drawback. Oka and Saito invented a Savart plate (SP) snapshot imaging polarimeter (SIP) whose principle can be analogous to a prism SIP [4,5]. The difference between them is that the SPs are placed at

the aperture plane rather than the image plane as is the prism SIP, which makes device assembly much easier. Principally, this device was based on a pair of optical Fourier transforms produced by a 4f imaging system. The SPs inserted at the first Fourier plane create polarization-dependent shearing on the wavefront; the second optical Fourier transform converts the wavefront shearing into linear phases that finally produce sinusoidal fringes that encode the Stokes vector. By implementing a standard Fourier analysis, the Stokes vector can be decoupled and reconstructed simultaneously. This snapshot ability eliminates the need for any movable part of the system.

Conceptually, the 4f length of the system is necessary to produce double Fourier transforms. A relatively lengthy system results. However, a geometric model of the system would prove that an essential reduction can be achieved. In addition, the SP's innate property to create the fringe frequency will allow us to further miniaturize the polarimeter to a centimeter. Here we first introduce the layout of the compact and miniature SIP. A geometric model to replace the original Fourier-transform model will be developed to prove the new scheme. We then illustrate the unique condition of the system to miniaturize the device. A ministructure will be simulated by means of a ray tracing technique to demonstrate

the validity of the miniature SIP. Finally, a portable SIP is fabricated and demonstrated by showing the experimental results.

2. Layout and Geometric Modeling

Figure 1 illustrates the optical layout of the miniature SIP, which contains two SPs that sandwich a half-wave plate (HWP) oriented at 22.5° and an analyzer oriented at 45° . The whole as a group is placed at the aperture plane of a single camera. The camera is equipped with a bandpass filter for quasi-monochromatic applications. Compared to the original 4 f system, the current structure eliminates any unwanted space between the two elements in front of the camera. It also benefits from the flexible zoom ability of a single camera. These two changes make the device compact and cost-effective.

The double-Fourier-transform model cannot be used to explain the current configuration. Instead, a geometric ray model was developed to prove the device's principle. First, the SP can be considered as a ray shearing element in which two orthogonal polarization rays, the ordinary (o) and extraordinary (e), experience parallel shearing from each other after propagating through the SP [6]. This shearing is crucial in that it creates a geometric optical path difference (OPD) between the o ray and the e ray that varies linearly with incident angle θ as illustrated by inset I in Fig. 1. With the imaging lens, the incident angle can be interpreted by the coordinates at the image plane. The combination of the two SPs and

HWP generates four output rays from a common incident ray, with equal and diagonal shearing as illustrated in inset II in Fig. 1. Note that the HWP at 22.5° rotates the electric field vector by 45° , enabling the second SP to shear the rays that exit from the first SP. At the end, the imaging lens recombines the four rays and the rays mutually interfere at the image plane. The resultant interferogram can be detected by the insertion of an analyzer at 45° .

The total irradiance at the image plane can be written as a sum of the four rays and their mutual interference:

$$I(x_i, y_i) = \left\langle \left| \frac{1}{2} E_y(x_i, y_i; t) e^{-i\phi_1} - \frac{1}{2} E_y(x_i, y_i; t) e^{-i\phi_2} + \frac{1}{2} E_x(x_i, y_i; t) e^{-i\phi_3} + \frac{1}{2} E_x(x_i, y_i; t) e^{-i\phi_4} \right|^2 \right\rangle, \quad (1)$$

where the bracket represents the time average, x_i and y_i are the coordinates of the image plane, each term within the brackets represents the electric field of a ray after it passes the analyzer, and ϕ_1 through ϕ_4 denote the accumulative phases of the individual ray paths. By unfolding Eq. (1) with proper arrangements, we can obtain

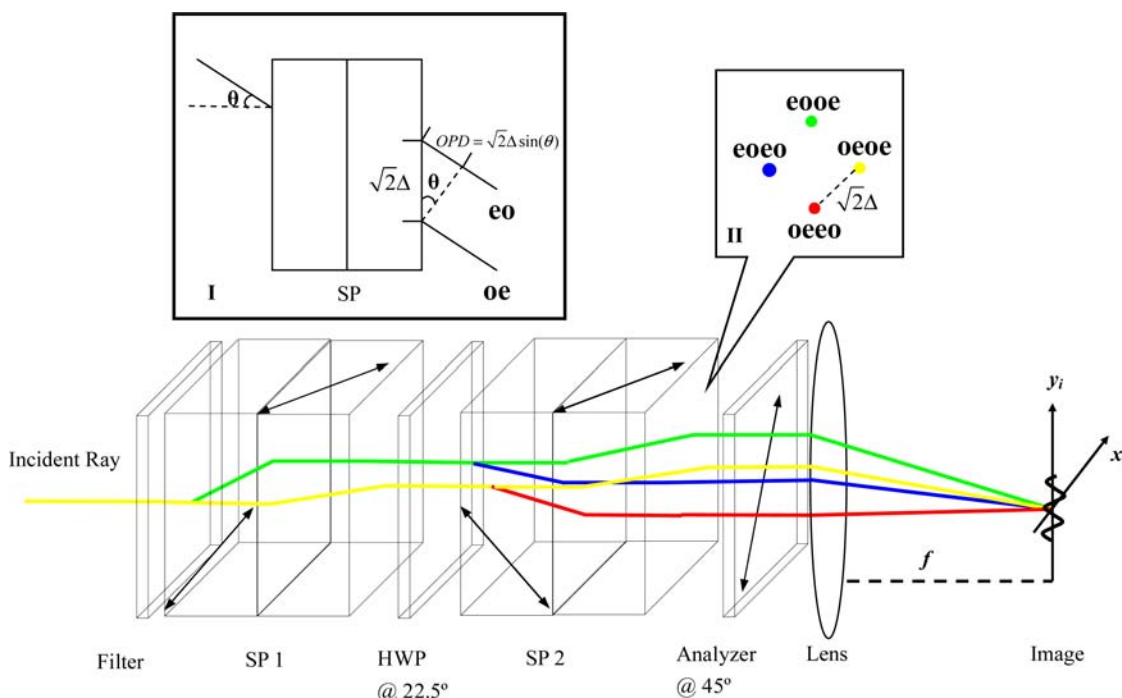


Fig. 1. (Color online) Optical layout of a miniature SIP. The double ended arrows, each tilting at 45° with respect to the edge of the surfaces, depict the optic axes of the calcite plates. Inset I, the OPD formation of a SP between two orthogonal polarization rays for a skewed incident ray. Inset II, the four emerging rays off the back surface of SP 2. The e and o denote the polarization consequences through the system.

$$\begin{aligned}
I = \frac{1}{4} \{ & 2[\langle |E_y|^2 \rangle + \langle |E_x|^2 \rangle] - [\langle |E_y|^2 \rangle e^{i(\phi_2 - \phi_1)} + c.c.] \\
& + [\langle |E_x|^2 \rangle e^{i(\phi_4 - \phi_3)} + c.c.] + [\langle E_x^* E_y \rangle e^{i(\phi_3 - \phi_1)} + c.c.] \\
& - [\langle E_x^* E_y \rangle e^{i(\phi_4 - \phi_2)} + c.c.] + [\langle E_x^* E_y \rangle e^{i(\phi_4 - \phi_1)} + c.c.] \\
& - [\langle E_x^* E_y \rangle e^{i(\phi_3 - \phi_2)} + c.c.] \}, \quad (2)
\end{aligned}$$

where variables x_i , y_i , and t are suppressed. Under ideal conditions, ϕ_1 through ϕ_4 can be written as spatially linear functions as

$$\begin{aligned}
\phi_1(x_i, y_i) = 0, \quad \phi_2(x_i, y_i) = 2\pi \frac{\Delta}{\lambda f} (x_i + y_i), \\
\phi_3(x_i, y_i) = 2\pi \frac{2\Delta}{\lambda f} x_i, \quad \phi_4(x, y) = 2\pi \frac{\Delta}{\lambda f} (x_i - y_i), \quad (3)
\end{aligned}$$

where λ is the wavelength and $\sqrt{2}\Delta$ represents the shearing distance generated by a SP. It is readily known that the following equations are valid [7]:

$$\begin{aligned}
\langle |E_x|^2 \rangle + \langle |E_y|^2 \rangle = S_0, \quad \langle |E_x|^2 \rangle = \frac{1}{2}(S_0 + S_1), \\
\langle |E_y|^2 \rangle = \frac{1}{2}(S_0 - S_1), \quad \langle E_x^* E_y \rangle = \frac{1}{2}(S_2 + iS_3). \quad (4)
\end{aligned}$$

By plugging Eqs. (3) and (4) into Eq. (2), we can finally arrive at the intensity pattern as

$$\begin{aligned}
I(x_i, y_i) = \frac{1}{2} S_0 + \frac{1}{2} S_1 \cdot \cos(2\pi\Omega(x_i + y_i)) \\
+ \frac{1}{4} |S_{23}| \cdot \cos[2\pi(2\Omega)x_i - \arg(S_{23})] \\
- \frac{1}{4} |S_{23}| i \cdot \cos[2\pi(2\Omega)y_i + \arg(S_{23})] \\
S_{23} = S_2 + iS_3, \quad \Omega = \frac{\Delta}{\lambda f}. \quad (5)
\end{aligned}$$

Note that in Eq. (5) the Stokes parameters S_1 through S_3 are modulated by various carrier frequencies, but S_0 remains a DC component. This fact allows us to decouple them in the frequency domain by implanting a Fourier transform and then recovering them simultaneously by inverse Fourier transformation [3].

This model convinces us that the new system formulates a linear combination of individual Stokes parameters in an image but in a much more compact layout. We need to mention that this model ignores any diffraction and aberration effects that can potentially affect the polarimeter's performance. An advanced aberration model will be developed elsewhere to address these profound issues [8].

3. Condition of Miniaturization

In addition to the system reduction, a unique property of the SP can make an additional contribution to the miniaturization of the device. The fringe fre-

quencies in Eq. (5), which we call the carrier frequencies (CFs), are proportional to $\Omega = \frac{\Delta}{\lambda f}$. For a calcite SP, the shearing distance $\sqrt{2}\Delta = 0.075t$ (μm), where t is the thickness in millimeters of the SP [6]. At a fixed wavelength and CFs (Ω), t is proportional to f , the focal length of the imaging lens. This becomes an important feature in that the total length of the polarimeter can be scaled by a common factor. If a miniature lens can be implemented, the whole device can be scaled down significantly. We use a cell phone camera as an example with $f = 5$ mm and pixel spacing of $4.75 \mu\text{m}$, $\lambda = 0.55 \mu\text{m}$, and $\Omega = 4$ pixels/fringe. The required thickness t then equals 1.54 mm and the total length of the polarimeter is shorter than 1.5 cm, which to our knowledge is the smallest imaging polarimeter to date. If we change the calcite to other higher birefringence materials, the size of the polarimeter can be made even smaller. Compared with other polarization elements, the plane-parallel feature of the SPs makes it more cost-effective in terms of fabrication and assembly.

4. Ray Tracing Analysis of a Miniature Snapshot Imaging Polarimeter

As a theoretical demonstration, the above-mentioned parameters of a miniature system are inserted into Zemax with a 5 mm diameter pupil. The image spot diagrams and ray shearing diagrams from this simulation are shown in Fig. 2. Two different field points are sampled, and the object is at a distance of 1 m for each field point. The image quality looks impressive

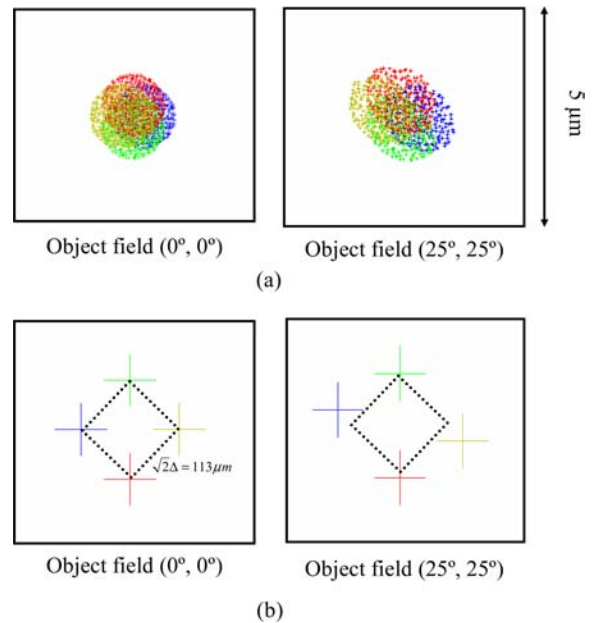


Fig. 2. (Color online) (a) Simulated image spot diagrams of a miniature SIP at best focus. The imaging lens was modeled as a paraxial lens. The object is 1 m away, and two field points $(0^\circ, 0^\circ)$ and $(25^\circ, 25^\circ)$ are sampled. The off-axis spot diagram displays anisotropy. (b) The ray shearing diagrams at the back surface of SP 2 for the $(0^\circ, 0^\circ)$ and $(25^\circ, 25^\circ)$ field points, respectively. For visual purposes, one incident ray is shown. The dotted rectangle is drawn to illustrate the diagonal shearing among the four rays.

for both the on-axis and the off-axis cases where the spot sizes of the image are close to the diffraction limit. This result diminishes the concern that the SPs could introduce excessive aberrations when imaging a finite conjugate object. In Fig. 2(b), the on-axis ray shearing diagrams are consistent with expectation, i.e., four rays are sheared equally and diagonally with values of $\sqrt{2}\Delta = 113\ \mu\text{m}$. Conversely, in the off-axis case, the four rays are not sheared ideally and their shearing distances are not equal to each other. Both are due to the retardance isotropy of the SP itself. This deviation deteriorates from an on-axis to an off-axis case, and it could undermine the sinusoidal nature of the fringes, producing errors in the reconstruction. Fortunately, our simulation indicates that such a deviation deteriorates slowly from the on-axis case to the off-axis case, and we determined that these errors can be calibrated by a reference image (see Section 5). Moreover, we also determined through simulation that the miniature SIP also works well over a large depth-of-focus range and a wide field of view.

5. Experimental Demonstration

For a proof-of-concept demonstration, we built a compact system with commercially available elements, all of which are 1 in. (2.54 cm) diameter and mounted independently. The SPs were manufactured by Karl Lambrecht Corporation, Chicago, Illinois. We used a 75 mm focal-length lens, which extended the total length of the system by a factor of 15 from its miniature counterpart. However, it still remains a portable size as seen in the photo of the polarimeter in Fig. 3.

Figure 4(a) shows a sample raw image obtained with the compact SIP; Fig. 4(b) shows the reconstructed Stokes images. A uniform polarized image is formed with a linear polarizer at 22.5° ($S_1 = 0.707$, $S_2 = 0.707$, $S_3 = 0$) to be used as a reference to calibrate the system. The camera's view angle is approximately 60 deg with respect to the ground, and the object, a car, is approximately 30 m away. In Fig. 4(a), the clear fringes seen across the image indicate the existence of polarization signals. This is due to the skewed Sun-object-camera angle and less scattering surfaces that are inside the scene. There is a change in the fringe pattern on various surfaces

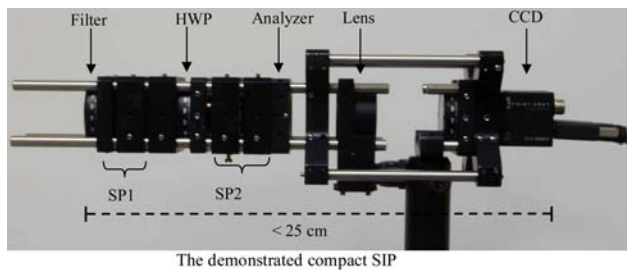


Fig. 3. Demonstrated compact SIP with a scaling factor of 15 from a miniature SIP. The CCD camera has a pixel spacing of $4.75\ \mu\text{m}$.

(e.g., the window) of the car, indicating that different SOPs are reflected. The reconstructed Stokes images in Fig. 4(b) also demonstrate this by clearly identifying the shape of the car in different Stokes parameters. We can see that the circular polarization (in S_3) is weaker than the linear polarization (S_1 and S_2). The region around the broken ground (below the car in the image) looks noisy, because it contains a higher frequency content that the processing algorithm cannot fully recover [3].

It is worth mentioning that, compared with a miniature SIP, the enlarged system suffers from larger aberrations. Aberrations degrade the camera performance in two ways: (1) introducing errors in the reconstruction, especially for off-axis fields and (2) washing out the fringe contrast [8]. With the current

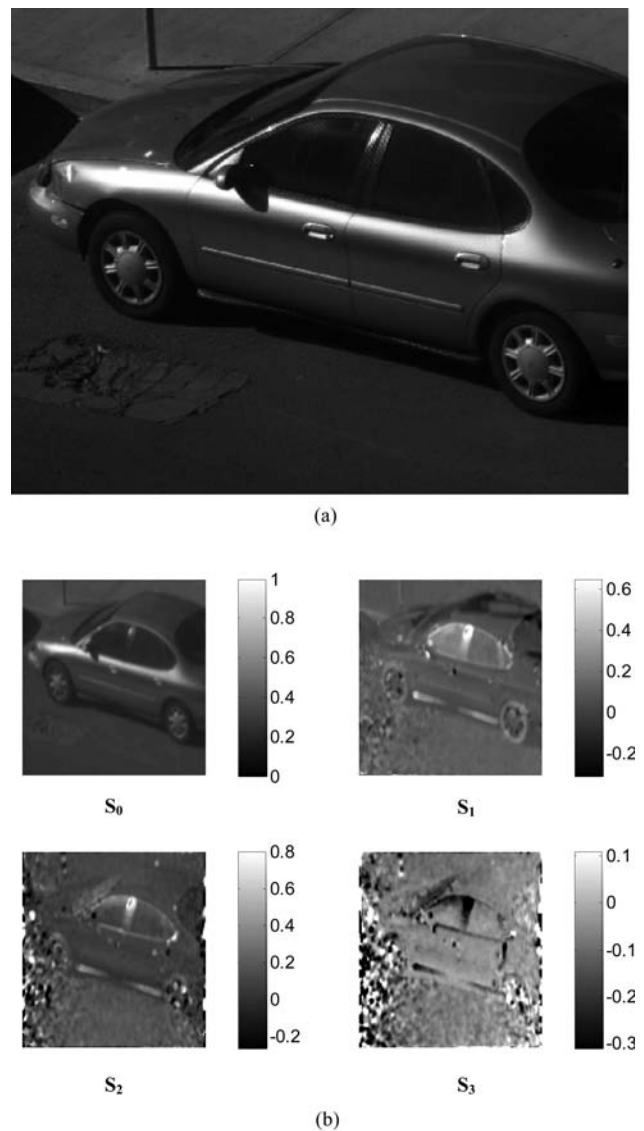


Fig. 4. (a) Raw image obtained with the compact SIP. A 3 nm bandwidth filter is used in front of the polarimeter. (b) Reconstructed Stokes images.

encouraging results, it is expected that better performance can be achieved with a miniature SIP.

6. Conclusions

In conclusion, we have demonstrated a compact snapshot imaging polarimeter by use of a group of functional polarization elements at the aperture plane. This approach is superior for making a miniature SIP that could open many applications for which polarization information is important. The simple configuration, easy alignment, and cost-effectiveness make this technique competitive. A proof-of-concept device has been fabricated to demonstrate the miniature SIP by showing both the numerical simulation and the real experimental results.

References

1. G. P. Nordin, J. T. Meier, P. C. Deguzman, and M. W. Jones, "Micropolarizer array for infrared imaging polarimetry," *J. Opt. Soc. Am. A* **16**, 1168–1174 (1999).
2. J. P. Guo and D. Brady, "Fabrication of thin-film micropolarizer arrays for visible imaging polarimetry," *Appl. Opt.* **39**, 1486–1492 (2000).
3. K. Oka and T. Kaneko, "Compact complete imaging polarimeter using birefringent wedge prisms," *Opt. Express* **11**, 1510–1519 (2003).
4. N. Saito and K. Oka, "Two-dimensional measurement of polarization using spatial carrier," in *Extended Abstracts of the 47th Spring Meeting of the Japan Society of Applied Physics and Related Societies* (Japan Society of Applied Physics, 2000), in Japanese.
5. K. Oka and N. Saito, "Snapshot complete imaging polarimeter using Savart plates," *Proc. SPIE* **6295**, 629508 (2006).
6. R. S. Sirohi and M. P. Kothiyal, *Optical Components, Systems, and Measurement Techniques*, (Marcel Dekker, 1991), Chap. 2, p. 68.
7. D. Goldstein, *Polarized Light*, 2nd ed. (Marcel Dekker, 2003), Chap. 4, p. 60.
8. H. T. Luo (College of Optical Science, University of Arizona, 1630 East University Boulevard, Tuscon, Arizona 85721, K. Oka and E. L. Dereniak are preparing a paper with the title of "Advanced model for simulating the polarization aberration in a compact Savart plate imaging polarimeter."